2023-08-30

Heat and mass transfer investigation of unsteady magnetohydro dynamic nanofluid flow in a porous pipe in the presence of chemical reactions

Zahor, Feda

Journal of Engineering and Technology Research

AJ ACADEMIC JOURNALS
expand your knowledge

Journal of Engineering and Technology Research

Full Length Research Paper

Heat and mass transfer investigation of unsteady magnetohydro dynamic nanofluid flow in a porous pipe in the presence of chemical reactions

Feda Abdalla Zahor[1]*, Ahmada Omar Ali[2], Reema Jain[3] and Verdiana Grace Masanja[1]

[1]The School of Computational and Communication Science and Engineering, The Nelson Mandela African Institution of Science and Technology (NM-AIST), Arusha, Tanzania.
[2]Department of Computer Systems and Mathematics, Ardhi University, Dar-es-Salam, Tanzania.
[3]Department of Mathematics and Statistics, Manipal University Jaipur, India.

This article presents a numerical investigation of mass and heat transfer effects on an unsteady Magnetohydrodynamic (MHD) nanofluid flow in a permeable pipe. The influences of the chemical reaction and magnetic flux are considered. With the central finite-difference technique, the fundamental equations are discretized. The resulting equations are solved numerically using methods of lines, bvp4, and shooting methods. The influences of material factors on the solution are investigated and displayed through tabular and graphical illustrations. The study revealed that the Sherwood number, skin friction, and rate of heat transfer are all decreased by an increase in the magnetic field. Additionally, the rate of rise of the chemical reaction and Brownian motion is observed to reduce the concentration of the nanofluid. Furthermore, the study finds that the Soret number, porosity medium resistance parameter, and thermophoresis parameter all cause the concentration profile to climb; while, increasing the pace of the chemical reaction and brown mobility leads the profile to decline.

Key words: Chemical reaction, porous medium, magnetohydrodynamic (MHD, nanofluid.

INTRODUCTION

Nanofluids are the type of fluid that contains ultrafine nanoparticles suspended in common fluids such as water, ethylene glycol, and propylene glycol. They are applied to improve these base fluids' thermal conductivity. In the same transfer of heat apparatus, Nanofluids are the type of fluid that contains ultrafine nanoparticles suspended in common fluids such as propylene glycol, ethylene glycol, and water. They are applied to improve these base fluids' thermal conductivity in the same heat transfer experiment; it was found that the thermal conductivity of nanofluids exceeded that of conventional fluids by threefold (Choi and Eastman, 1995). The

*Corresponding author. E-mail: fedaz@nm-aist.ac.tz.

transfer of heat and flow properties of nanofluids has been studied in many investigations.

Khan and Pop (2010) observed that the decreased Nusselt number declines while the reduced Sherwood number increases when the Prandtl number, thermophoresis parameter, and Brownian motion parameter grow. High Lewis and Rayleigh numbers result in the homogeneity of nanoparticle dispersion, as demonstrated by Kuznetsov and Nield (2010) in their study. In a partially open trapezoidal cavity, Sheremet et al. (2018) investigated the natural convection of water-based nanofluids under Brownian diffusion and thermophoresis. In their examination of the magnetohydrodynamic physical phenomenon, the flow of nanofluids across an exponentially stretched sheet, Reddy et al. (2019) came to the conclusion that as the parameter for the viscous ratio is increased, the coefficient of skin friction falls. In their study of the effects of nanoparticle slip mechanisms on the inherent heat transfer properties of nanofluids in an enclosure (Amidu et al., 2021) studied the influence of the causes of nanoparticle slip on nanofluids' characteristics of natural heat transfer in an enclosure, concluding that thermophoresis diffusion enhances the transfer of heat. Khan et al. (2022) investigated the behavior of a squeezing flow of hybrid nanoparticles in the presence of an electric field. The results showed that increasing the value of the suction/injection parameter resulted in a gradually opposite behavior of the velocity profile.

The heat transfer process through unsteady Magnetohydrodynamic (MHD) flow over various surfaces has garnered significant importance recently (Dhanalaxmi, 2015). The research investigated the impact of heat and viscous dissipation on an unsteady MHD flow over an extended surface. The results of the study revealed that with an increase in magnetic parameters, both the Nusselt number and the skin friction decreased. Makinde et al. (2019) studied the impacts of the heat source on an unsteady MHD inflow of a non-Newtonian nanofluid in a permeable medium. The findings demonstrated that as magnetic parameters are increased, the Grashof and Nusselt number drop. The rate of constant laminar of magnetohydrodynamic fluid via a permeable pipe bedded in a previous material was studied by Barik et al. (2018). They found that as the magnetic and porosity parameter values rise, axial haste diminishments. The inspiration of MHD on heat radiation in free convection flow via a perpendicular plate has been investigated by Abdullah et al. (2019). The findings indicate that MHD's impact on fluid flow arises as a magnetic parameter effect. The magnetic field causes a decrease in the flow of the fluid. Additional research can be located in the works of Zubaidah and Kechil (2019) as well as Khan and Rashad (2017). Sharma et al. (2023) used response surface methods to investigate the heat transfer rate of MHD nanofluid blood flow via a stenosed composite artery with

hematocrit-dependent viscosity and the Hall effect. The results reveal that when the Hall parameter grows, the Nusselt number drops, indicating that heat transmission reduces as electromagnetic force increases. Saeed et al. (2022) investigated the theoretical study of the physical properties of an unsteady, squeezing nanofluid. The thermophoresis and Brownian motion play critical roles in the nanofluid concept. The result showed that when the squeezing number is reduced, the velocity and temperature profiles increase, while the concentration profile drops. It further demonstrated that when the Prandtl number increases, the temperature profile drops, whereas the concentration profile exhibits the reverse trend.

Arulmozhi et al. (2022) investigated the effects of thermal radiation and chemical reactions on the MHD free convective heat and mass transfer effects of a nanofluid on an infinite moving upright plate. The results demonstrated that as the volume proportion of the solid particle grows, so does the velocity.

Engineers and scientists benefit significantly from the study of mass transfer and heat. This is due to its widespread usage in many fields of science and engineering, including thermal energy storage, plastic melting, solar collectors, paper manufacture, engine cooling, etc. (Elbashbeshy et al., 2018) studied the numerical transfer rate of heat and mass through a stretched area with different values of thickness buried in a permeable medium using a Maxwell nanofluid.

Keshtkar and Ghazanfari (2017) discussed the impact of a magnetic field on fluid flow and transfer of heat inside a 2D enclosure. They come to the conclusion that as the Darcy number rises; permeability naturally rises, increasing convective heat transfer.

Boukerma and Kadja (2017) investigated the impact of ethylene glycol-base, CuO and $Al_2 O_3$ nanofluids on the heat transmission in a cylinder. They reveal that the coefficient of transfer of heat rises along with the nanoparticle size and Reynolds number. Haile and Shankar (2014) and Humane et al. (2021) analyzed the transmission of heat and mass in the boundary film stream of an unstable viscid fluid across a stretched pane in the presence of radiation, chemical reaction, heat production, and magnetic field. The results reveal that the unsteady flow exhibits a coefficient skin friction, mass, and heat transmission rate that is greater than the equivalent fragments of the numbers under steady-state conditions.

Also, Mahabaleshwar et al. (2021) investigated the impacts of a stretching/shrinking sheet on an angled magnetic field, as well as heat transmission of an MHD fluid. The results establish that the growth in the radiation promotes heat diffusion, which causes the temperature to rise through the laminar boundary layer. Muyungi et al. (2022) investigated how Navier's boundary condition and skin friction affected the movement of a nanofluid in a

permeable pipe. They establish that the increasing Reynolds amount increases temperature and velocity. However, a rise in the Navier slip parameter leads to a drop in temperature and a slowing of velocity. Mjankwi et al. (2019) used unsteady MHD to examine the flow of a nanofluid with different properties of the fluid as it ran over an inclined stretched sheet in the existence of chemical processes and radiation. They took into account the impact of fluid characteristics on diffusion coefficient and thermal conductivity. The findings imply that concentration declines as the chemical reaction constraint increases.

Due to its application in several industries, including chemical, power, cooling, flow in a desert cooler, and other uses, it is crucial to investigate how chemical reactions affect the transfer of heat and mass stream. Das et al. (2020) studied the MHD boundary layer drift, and heat transfer characteristics of nanofluids across a stretched sheet in a permeable medium. The results show that a decrease in diffusion is implied by an augmentation of the chemical reaction variable in the flowing ground, which lowers the velocity and temperature profiles. Kandasamy et al. (2006) explored the influences of heat, mass transfer, and chemical processes, on natural convection near a porous wedge surface considering suction or injection. After investigation, the findings reveal that in the existence of homogeneous heat radiation, fluid concentration rises as the chemical reaction intensifies while fluid velocity and temperature fall. Additionally, they draw the conclusion that skin friction is observed to grow as chemical reaction rises in suction and injection. Arifuzzaman et al. (2018) investigated the impacts of mass diffusion, radiation, and transfer of heat, on the unsteady fluid flow through a vertical permeable plate. They observe that whereas concentration profiles decrease with an increase in chemical reaction parameters, the order of chemical reaction parameters rises. Rao and Deka (2023) investigated the heat and mass transport of a Williamson nanofluid flowing in a two-dimensional, unstable MHD flow over a porous, vertically moving cylinder. The findings showed that while increases in the Prandtl number had the opposite impact, increases in the Brownian motion, thermophoresis, and radiation parameters all result in a higher temperature profile for the nanofluid. The constant flow of convective fluid through a porous region with a diffusion-thermo was investigated by Obulesu et al. (2021). The findings demonstrate that the temperature declines with increasing Prandtl quantity, radiation, and Heat source specification. The impact of the magnetic field, thermal radiation, permeable media, and chemical reaction on the heat and mass transfer of a steady, laminar, and 2D nanofluid flow was investigated by Sadighi et al. (2022). The results demonstrate that by increasing viscous dissolution, the nanofluid efficiency is increased by absorbing heat from

the thermal boundary layer. Recent years have seen continued interest in this area of review (Nayak et al., 2016; Aly et al., 2020).

Innovation across a range of areas was the inspiration for this inquiry. There are currently no published studies in the consulted literature on the concept of the mass and heat transfer effect in an unstable MHD nanofluid flow through a pipe filled with porous materials of uniform porosity while taking an externally applied, strong radial magnetic field into consideration.

Design of a mathematical model

Figure 1 shows how the problem that was the subject of this article is configured. Considered to be an unstable flow is the two-dimensional inflow of an electrically conducting, viscous, incompressible, laminar fluid along the direction chosen as the axis of a permeable pipe. A constant-intensity magnetic field is also applied vertically to the pipe as a chemical reaction also occurs.

The following equations are responsible for governing the flow of the fluid:

$$\frac{\partial u}{\partial z} = 0. \tag{1}$$

$$\frac{\partial u}{\partial t^*} + V\frac{\partial u}{\partial r} = -\frac{1}{\rho}\frac{\partial p}{\partial r} + \frac{\mu}{\rho}\frac{1}{r}\frac{\partial}{\partial r}\left(r\frac{\partial u}{\partial r}\right) - \frac{\sigma_f B_0^2 u}{\rho} - \frac{\mu}{\rho K} - \frac{F}{\rho\sqrt{K}}u^2. \tag{2}$$

$$\frac{\partial T}{\partial t^*} + V\frac{\partial T}{\partial r} = \frac{k}{\rho c_p}\frac{1}{r}\frac{\partial}{\partial r}\left(r\frac{\partial T}{\partial r}\right) + \frac{\mu}{\rho c_p}\left[\left(\frac{\partial u}{\partial r}\right)^2 + \frac{u^2}{K}\right] + \frac{\sigma B_0^2 u^2}{\rho c_p} + \frac{F}{\rho c_p\sqrt{K}}u^3 + \tau\left[D_B\frac{\partial T}{\partial r}\frac{\partial C}{\partial r} + \frac{D_T}{T_\infty}\left(\frac{\partial T}{\partial r}\right)^2\right]. \tag{3}$$

$$\left(\frac{\partial C}{\partial t^*} + V\frac{\partial C}{\partial r}\right) = D_B\frac{1}{r}\frac{\partial}{\partial r}\left(r\frac{\partial C}{\partial r}\right) + \frac{D_T}{T_\infty}\left(\frac{\partial^2 T}{\partial r^2}\right) - K_r(C - C_\infty) \tag{4}$$

The initial and boundary conditions for the present problem are as follows:

$$u(r,0) = 0, \ T(r,0) = T_\infty, C(r,0) = C_w \quad \text{for } r \geq 0. \tag{5}$$

$$\frac{\partial u}{\partial r}(0,t^*) = \frac{\partial T}{\partial r}(0,t^*) = \frac{\partial C}{\partial r}(0,t^*) = 0 \quad \text{for } t^* > 0 \tag{6}$$

$$\left.\begin{array}{l} u(R,t^*) = 0, D_B\frac{\partial C}{\partial r}(R,t^*) = -\frac{D_T}{T_\infty}\frac{\partial T}{\partial r}(R,t^*), \\ -k_{nf}\frac{\partial T}{\partial r}(R,t^*) = h[T(R,t^*) - T_\infty]. \end{array}\right\} \tag{7}$$

The following non-dimensional quantities and parameters are introduced;

$$u = 0, v = V, k\frac{\partial T}{\partial r} = h(T - T_\infty), C = \text{Porous medium}$$
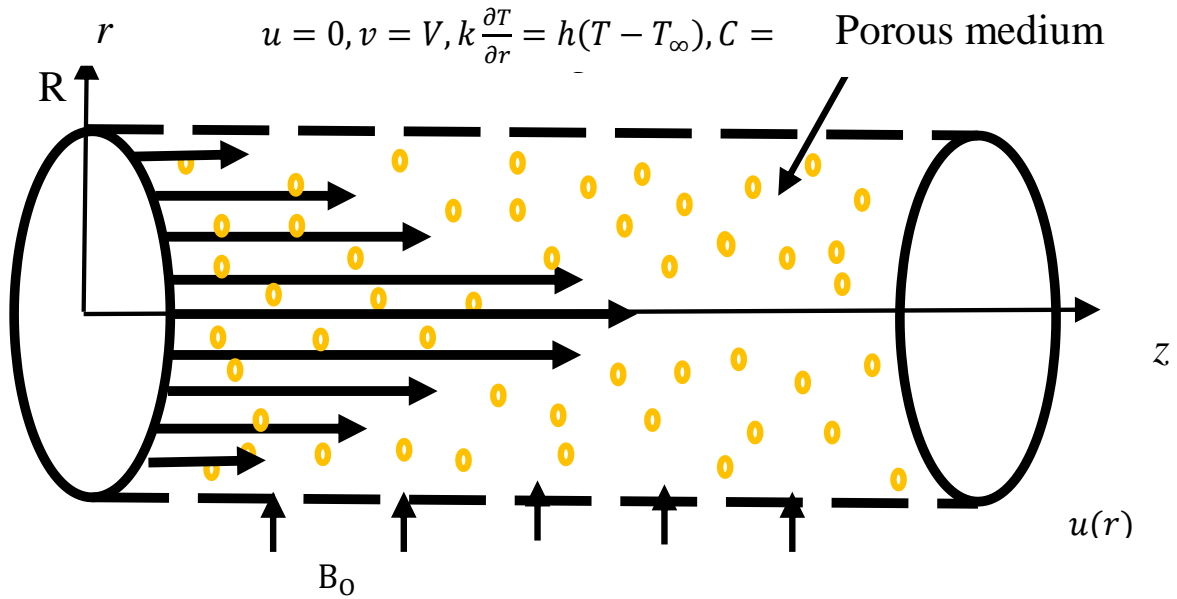
Figure 1. An illustration of the problem's schematic.

$$\theta = \frac{T - T_\infty}{T_w - T_\infty}, \varphi = \frac{C - C_\infty}{C_w - C_\infty}, \; W = \frac{u}{V}, \eta = \frac{r}{R}, Sc = \frac{\nu}{D_B},$$

$$t^* = \frac{t\nu}{R^2}, Z = \frac{z}{R}, P = \frac{Rp}{\mu_f V}, \tau = \frac{(\rho c_p)_n}{\rho c_p}, Re = \frac{VR}{\nu}, Bi = \frac{hD}{k}$$

$$M^2 = \frac{\sigma B_0^2 R^2}{\mu}, N_p = \frac{K}{R^2}, Pr = \frac{\mu c_p}{k} . K_R = \frac{K_r R^2}{\nu},$$

$$N_t = \frac{\tau D_T(T_w - T_0)}{T_\infty \nu}, N_b = \frac{\tau D_b(C_w - C_0)}{\nu}, A = -\frac{\partial P}{\partial \eta},$$

$$Sr = \frac{D_T(T_w - T_0)}{\nu T_\infty(C_w - C_0)}, Ec = \frac{V^2}{c_p(T_a - T_0)}, N_F = \frac{FR}{\rho\sqrt{K}} .$$ (8)

Substituting the dimensionless parameters of Equation 8 in Equations 1 to 7, results in Equations 9 to 15;

$$\frac{\partial W}{\partial Z} = 0.$$ (9)

$$\frac{\partial W}{\partial t} + Re\frac{\partial W}{\partial \eta} = A + \frac{1}{\eta}\frac{\partial W}{\partial \eta} + \frac{\partial^2 W}{\partial \eta^2} - (M^2 + N_p)W - ReN_F W^2$$ (10)

$$\frac{\partial \theta}{\partial t} + Re\frac{\partial \theta}{\partial \eta} = \frac{1}{Pr}\left(\frac{1}{\eta}\frac{\partial \theta}{\partial \eta} + \frac{\partial^2 \theta}{\partial \eta^2}\right) + N_b\frac{\partial \theta}{\partial \eta}\frac{\partial \varphi}{\partial \eta} + N_t\left(\frac{\partial \theta}{\partial \eta}\right)^2$$
$$+ Ec\left[\left(\frac{\partial W}{\partial \eta}\right)^2 + EcM^2, + EcN_p W^2 + N_F W^3\right]$$ (11)

$$\frac{\partial \varphi}{\partial t} + Re\frac{\partial \varphi}{\partial \eta} = \frac{1}{Sc}\left(\frac{1}{\eta}\frac{\partial \varphi}{\partial \eta} + \frac{\partial^2 \varphi}{\partial \eta^2}\right) + Sr\frac{\partial^2 \theta}{\partial \eta^2} - K_R\varphi$$ (12)

$$\theta(\eta, 0) = W(\eta, 0) = 0, \quad \varphi(\eta, 0) = 1, \quad \text{for } \eta \geq 0$$ (13)

$$\frac{\partial \theta}{\partial \eta}(0, t) = \frac{\partial W}{\partial \eta}(0, t) = \frac{\partial \varphi}{\partial \eta}(0, t) = 0, \text{for } t > 0$$ (14)

$$W(1, t) = 0, \frac{\partial \theta}{\partial \eta}(1, t) = -Bi\theta(1, t), \\ \frac{\partial \varphi}{\partial \eta}(1, t) = -\frac{N_t}{N_b}\frac{\partial \theta}{\partial \eta}(1, t) \Bigg\}$$ (15)

The Equation 16 provides the skin friction (C_f) and Nusselt number (Nu), and Sherwood number (Sh) as crucial physical parameters that must be considered in this study:

$$Nu = \frac{Rq_w}{k(T_w - C_\infty)}, C_f = \frac{R\tau_w}{\mu V}, Sh = \frac{Rq_m}{D_B(C_w - C_\infty)}$$ (16)

Where q_m and q_w are mass and heat fluxes at the surface respectively and τ_w is the wall shear stress. They are defined as in Equation 17:

$$\tau_w = \mu\frac{\partial u}{\partial r}\Big|_{R=r}, q_w = k\frac{\partial T}{\partial r}\Big|_{R=r}, q_m = D_B\frac{\partial C}{\partial r}\Big|_{R=r}$$ (17)

Thus,

$$\left. \begin{array}{l} C_f = \frac{\partial W}{\partial \eta} \\ Nu = \frac{\partial \theta}{\partial \eta} \\ Sh = \frac{\partial \varphi}{\partial \eta} \end{array} \right\} \text{ at } \eta = 1$$ (18)

Table 1. Comparison value of dimensionless velocity and dimensionless concentration function by three different schemes.

η	dimensionless velocity function W			dimensionless concentration function φ		
	Methods of lines	bvp4c	Shooting	Methods of lines	bvp4c	Shooting
0	0	0	0	1.576953	1.576954	1.576830
0.1	0.173305	0.173305	0.173322	1.577151	1.577153	1.577029
0.2	0.167512	0.167512	0.167529	1.577743	1.577744	1.577621
0.3	0.158107	0.158107	0.158123	1.578725	1.578727	1.578603
0.4	0.145247	0.145247	0.145263	1.580096	1.580098	1.579974
0.5	0.129052	0.129051	0.129065	1.581854	1.581855	1.581731
0.6	0.109606	0.109606	0.109617	1.583996	1.583997	1.583873
0.7	0.086965	0.086960	0.086973	1.586521	1.586523	1.586399
0.8	0.061155	0.061155	0.061161	1.58943	1.589431	1.589307
0.9	0.032175	0.032175	0.032178	1.59272	1.592721	1.592597
1	0	0	0	1.596392	1.596394	1.596269

NUMERICAL METHOD

The non-linear Equations 10 to 12 with initial and boundary conditions. Equations 13 to 15 are discretized into finite-difference equations using central finite-difference schemes. The approximate set of the finite-difference equations corresponding to Equations 9 to 15 are Equations 19 to 21:

$$\frac{dW_i}{dt} = A + \frac{W_{i+1}-W_{i-1}}{2\eta_i\Delta\eta} + \frac{W_{i+1}-2W_i+W_{i-1}}{(\Delta\eta)^2}$$
$$-Re\frac{W_{i+1}-W_{i-1}}{2\Delta\eta} - (M^2+N_p)W_i - N_F W_i^2 \qquad (19)$$

$$\frac{\partial\theta_i}{\partial t} = \frac{1}{Pr}\left(\frac{\theta_{i+1}-\theta_{i-1}}{2\eta_i\Delta\eta} + \frac{\theta_{i+1}-2\theta_i+\theta_{i-1}}{(\Delta\eta)^2}\right)$$
$$+N_b\frac{(\theta_{i+1}-\theta_{i-1})(\varphi_{i+1}-\varphi_{i-1})}{4(\Delta\eta)^2} + N_t\left(\frac{\theta_{i+1}-\theta_{i-1}}{2\Delta\eta}\right)^2$$
$$-Re\frac{\theta_{i+1}-\theta_{i-1}}{2\Delta\eta} + Ec\left(\frac{W_{i+1}-W_{i-1}}{2\Delta\eta}\right)^2 + EcM^2W_i^2 + EcN_pW_i^2 + EcN_FW_i^3 \qquad (20)$$

$$\frac{d\varphi_i}{dt} = \frac{1}{Sc}\frac{\varphi_{i+1}-2\varphi_i+\varphi_{i-1}}{(\Delta\eta)^2} + Sr\left(\frac{\varphi_{i+1}-\varphi_{i-1}}{2\eta_i\Delta\eta} + \frac{\theta_{i+1}-2\theta_i+\theta_{i-1}}{(\Delta\eta)^2}\right)$$
$$-Re\frac{\varphi_{i+1}-\varphi_{i-1}}{2\Delta\eta} - K_R\varphi_i \qquad (21)$$

With initial condition

$$W_i(0) = 0, \theta_i(0) = 0, \varphi_i(0) = 1 \text{ for } 1 \le i \le N+1. \qquad (22)$$

Where Equations 23 and 24 are adjusted to include the boundary, conditions specified in the first and last grid points' corresponding equations:

$$W_2 = W_1, \theta_2 = \theta_1, \varphi_2 = \varphi_1. \qquad (23)$$

$$\left.\begin{array}{l} W_{N+1} = 0, \theta_{N+1} = \theta_N(1-Bi\Delta\eta), \\ \varphi_{N+1} = \varphi_N - N_t\frac{\theta_{N+1}-\theta_N}{N_b} \end{array}\right\} \qquad (24)$$

The discretized form of the skin friction, Nusselt, and Sherwood figures are given by Equation 25:

$$Nu = \frac{\theta_{N+1}-\theta_N}{\Delta\eta}, Sh\frac{\varphi_{N+1}-\varphi_N}{\Delta\eta}, C_f\frac{W_{N+1}-W_N}{\Delta\eta} \qquad (25)$$

The technique of Runge-Kutta-Fehlberg integration was employed to iteratively resolve the set of basic differential equations with nonlinear solution (Equations 19 to 21 and 25) with known initial condition and boundary constraints (Equation 22 to 24) which were executed by a computer using MATLAB codes.

RESULTS AND DISCUSSION

Using the method of lines, a numerical solution is provided for the estimated outcome of the nonlinear model (Equations 9 to 11) under the initial and boundary conditions (Equations 13 to 15). The parameter values utilized in this research, unless otherwise specified are $N_p = 0.1, N_F = 0.1, N_b = 1, N_t = 1, Sc = 0.1. Sr = 0.6, K_R = 0.5, Pr = 6.2, M = 1, Re = -1, Ec = 0.1, A = 1$ and $Bi = 5$.

The impact of several characteristics, such as Nusselt and Sherwood amount, and skin friction for numerous values of material properties, on concentration, temperature, and velocity profiles are analyzed and discussed.

Additionally, apart from the method of lines, we have conducted a comparative analysis of two alternative numerical schemes at steady state, namely the bvp4c and shooting method, to validate and check the precision of code execution as illustrated in Table 1.

The fluid velocity profiles are depicted in Figures 2 to 5 to demonstrate the impact of various physical characteristics. As can be seen in Figures 2 and 3, the fluid velocity across the channel increases as the pressure gradient and porosity medium resistance parameter increase, whereas Figures 4 and 5 illustrate the opposite consequence of the magnetic constraint and Reynolds number on the fluid velocity. This is expected since the Lorentz and injection forces usually cause the
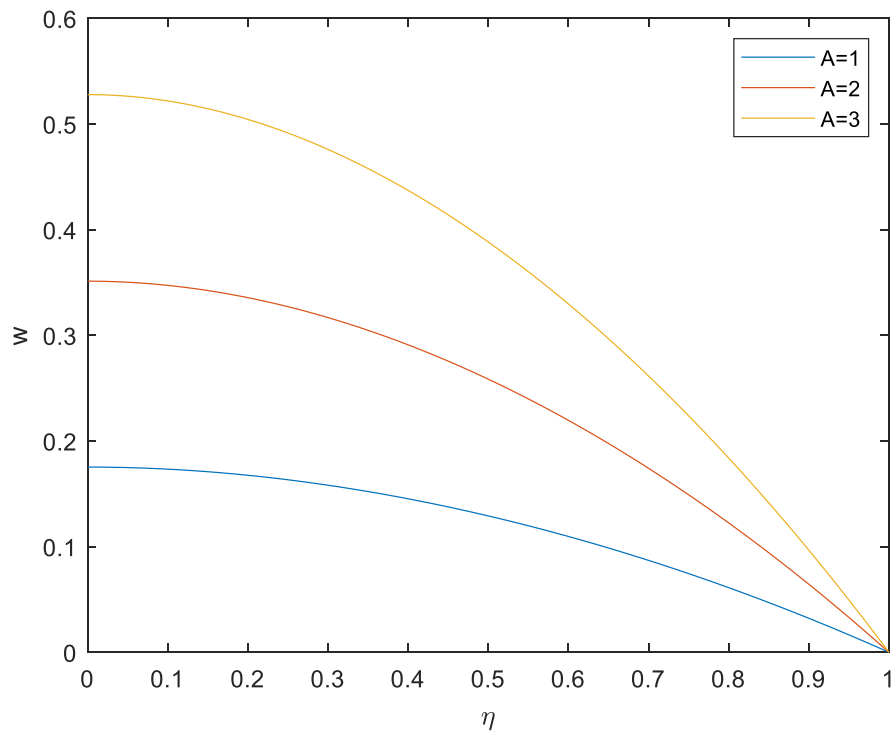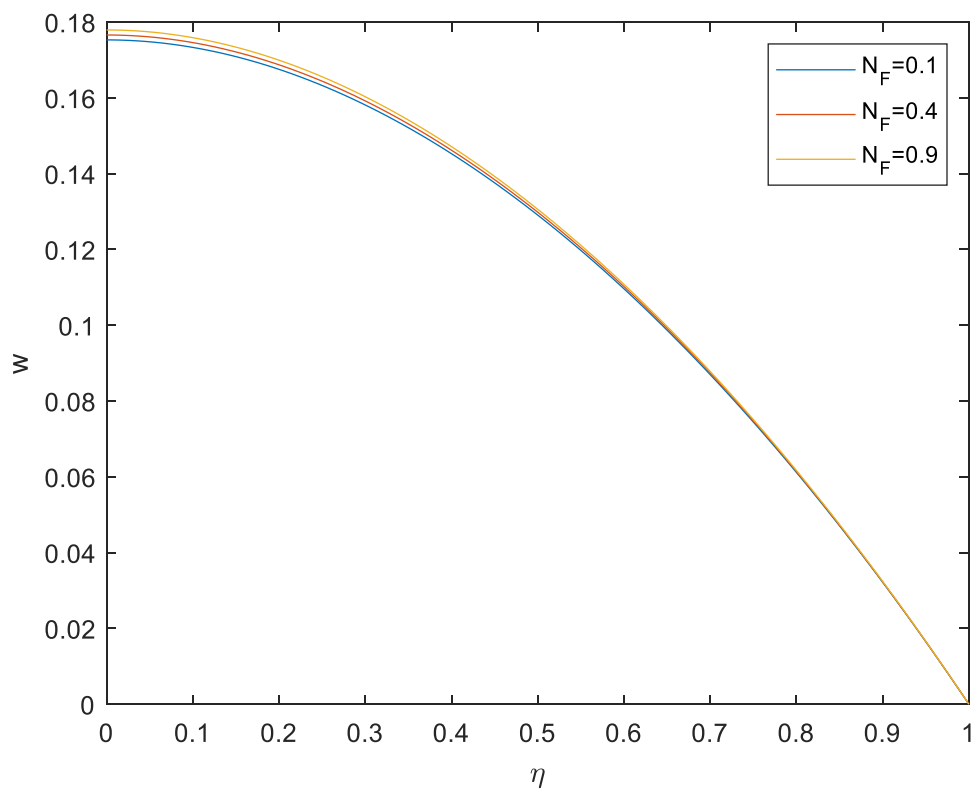
Figure 1. The influences of A on W.
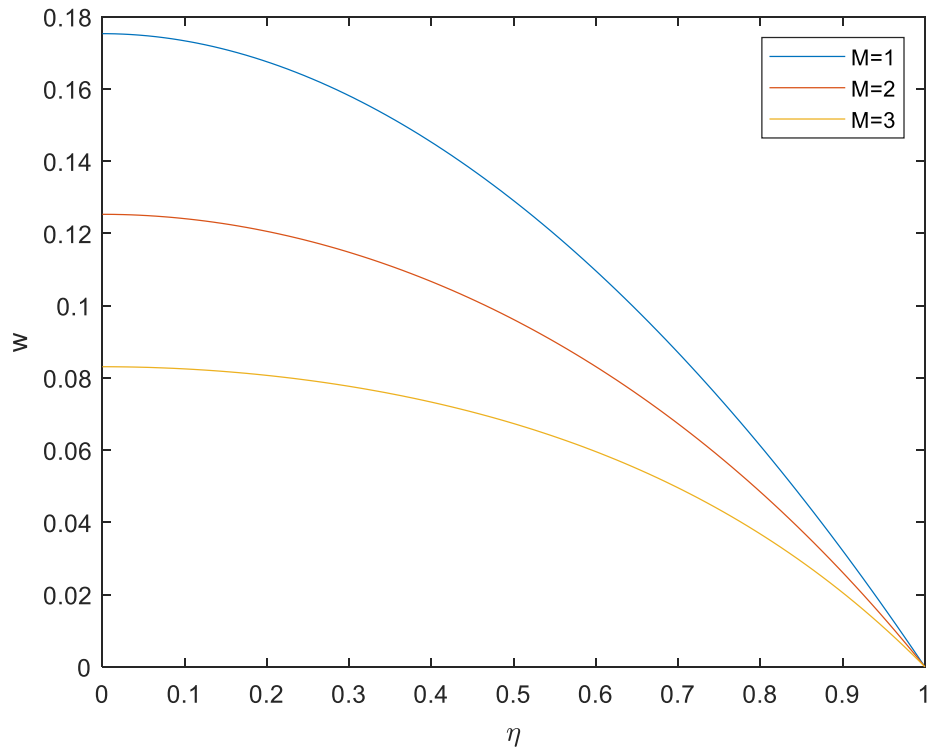

Figure 2. The impact of N_F on W.
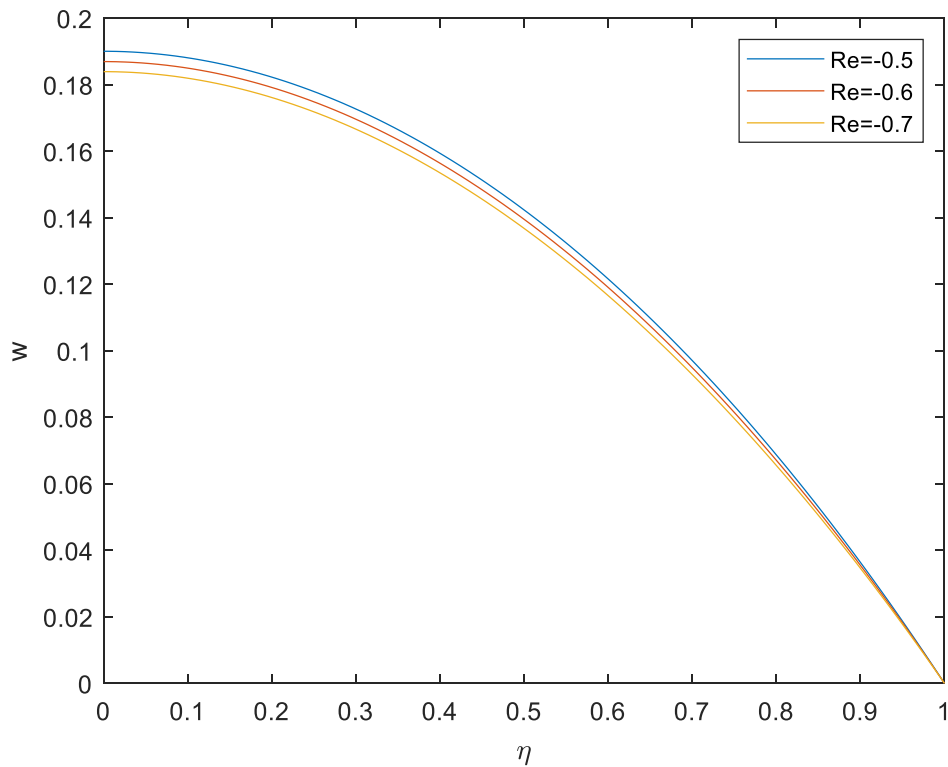
Figure 3. The effect of   M on W.

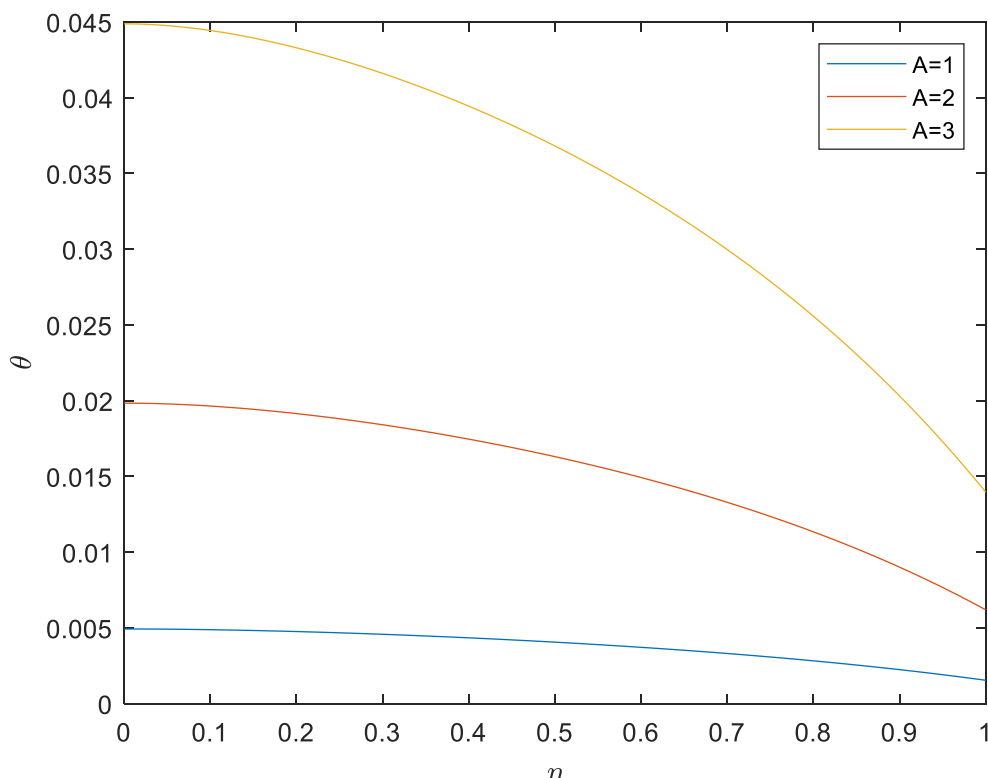**Figure 4.** The effect of Re on the W.

Figure 5. Distributions of temperature for varied values of A.

flow rate of the nanofluid to slow down.

Figures 6 and 7 illustrate the effect of pressure gradient and porosity medium resistance parameter on the temperature profile. These two parameters are observed to proportionally raise the temperature of the fluid as they are increased. In contrast, as observed in Figures 8 to 9, the fluid temperature cools down when the convection rate at the pipe wall and injection force parameter is increased. Therefore, by increasing the injection force and convection rate along the pipe wall, the system's thermal efficiency can be improved. The concentration profile of nanoparticles is affected by various physical parameters, as illustrated in Figures 10 to 14. It is noted that an increase in the molar mass diffusivity, coefficient of thermophoresis diffusion, and the flow system's nanoparticle concentration rises as a result of the porous medium's permeability. Conversely, the chemical reaction and Brownian motion of fluid particles are observed to decrease the fluid concentration due to the dispersion caused by raising the values of the constraints.

The impact of the magnetic field on Sherwood and Nusselt numbers and skin friction is presented in Figures 15 to 17.

In response to an upsurge in suction force, results in a growth in the Nusselt, and Sherwood numbers and skin friction, whereas the raising in the magnetic field produces the opposite effect.

Conclusion

An analysis has been made of the effects of temperature and mass transfer for an unsteady magnetohydrodynamic (MHD) nanofluid flow that is reacting to chemicals in a flexible pipe. The impacts of magnetohydrodynamics and thermal radiation have been observed. The fourth-order Runge-Kutta-Fehlberg method was employed for solving the transformed system of equations. The following list of major observations relates to the completed study:

1) The higher values of the pressure gradient and porosity medium resistance parameters boost the temperature and velocity profiles within the system.
2) Higher values of the Reynolds number and magnetic parameter result in a reduction of the profiles of velocity and temperature.
3) The Soret number, porosity medium resistance parameter, and thermophoresis parameter all cause the concentration profile to rise; however, increasing the rate of the chemical reaction and brown mobility causes the profile to fall.
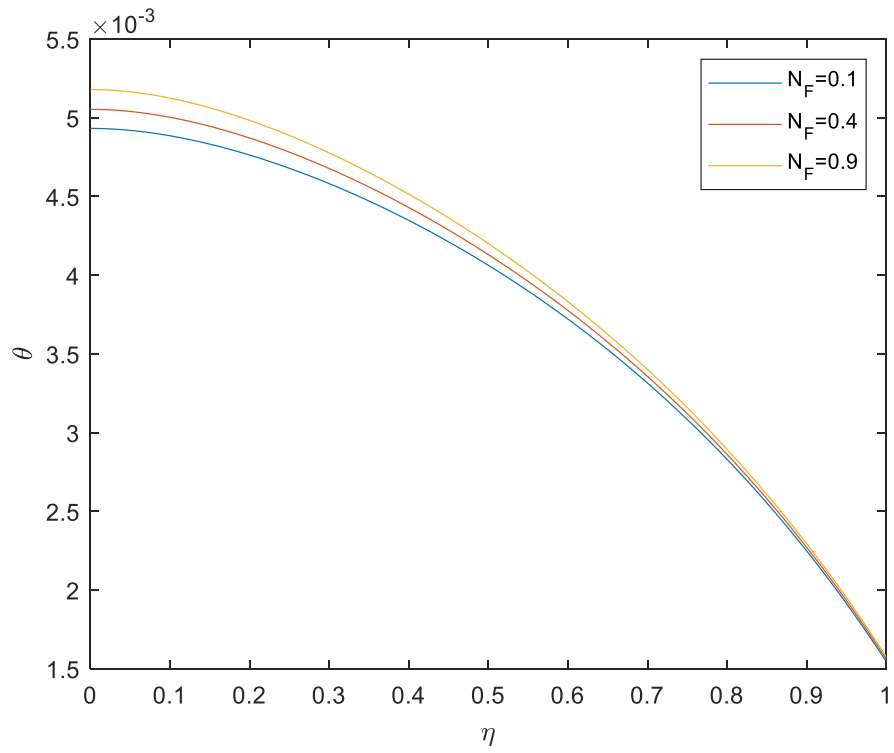
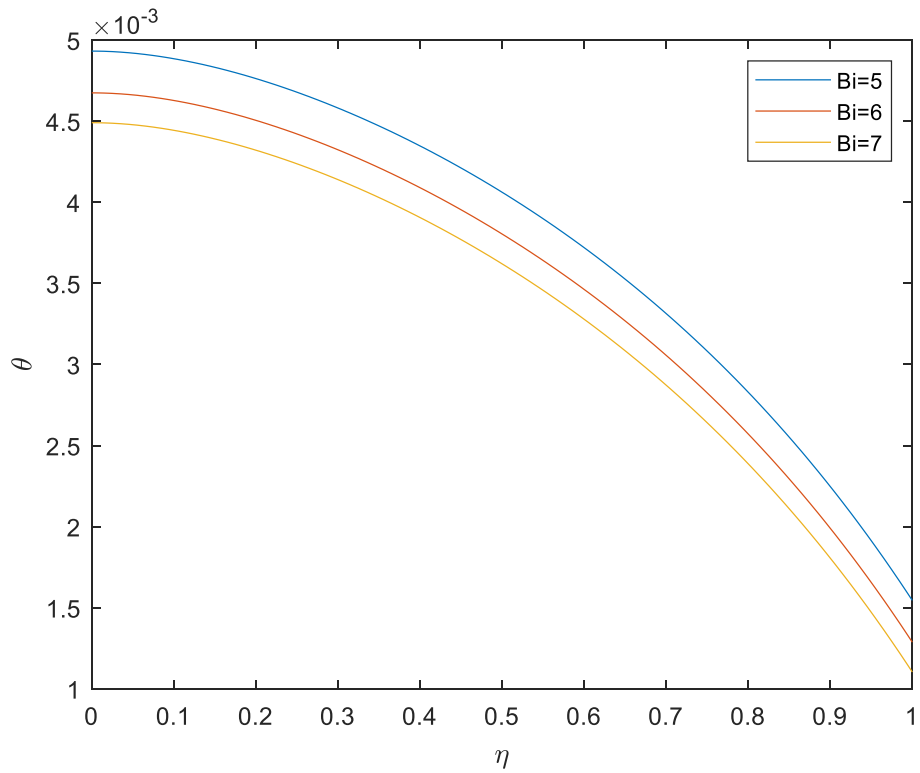**Figure 6.** Distributions of temperature for several values of N_F.

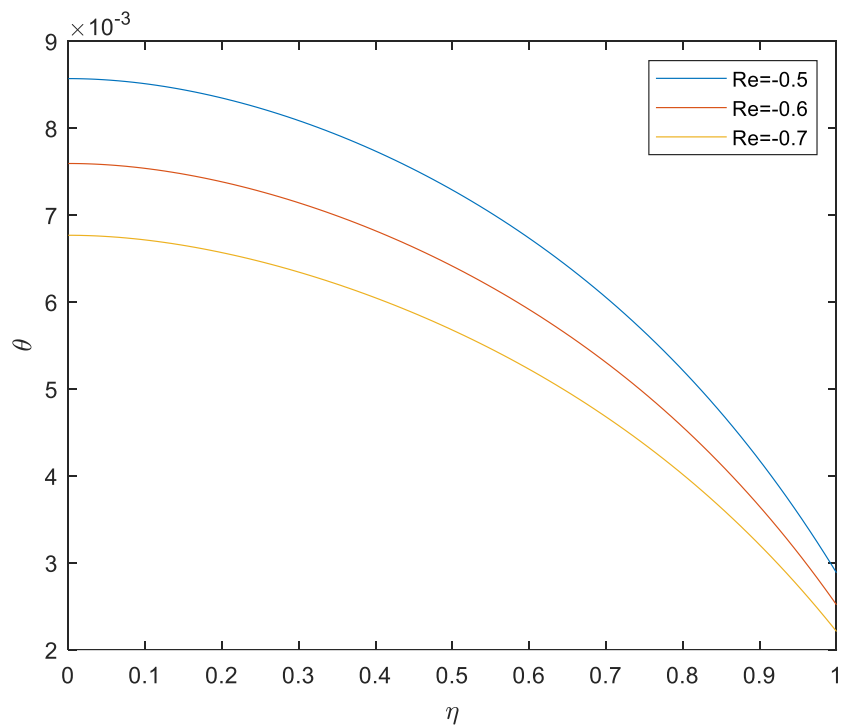**Figure 7.** Distributions of temperature for various values of Bi.

Figure 8. Distributions of temperature for numerous values of Re.
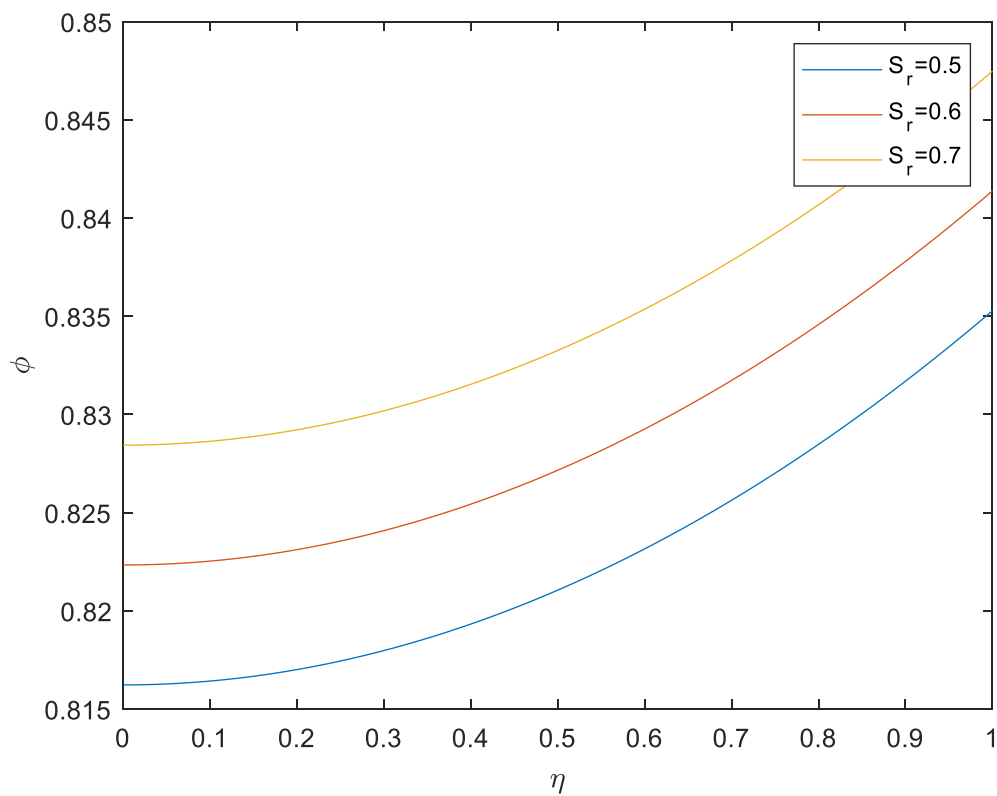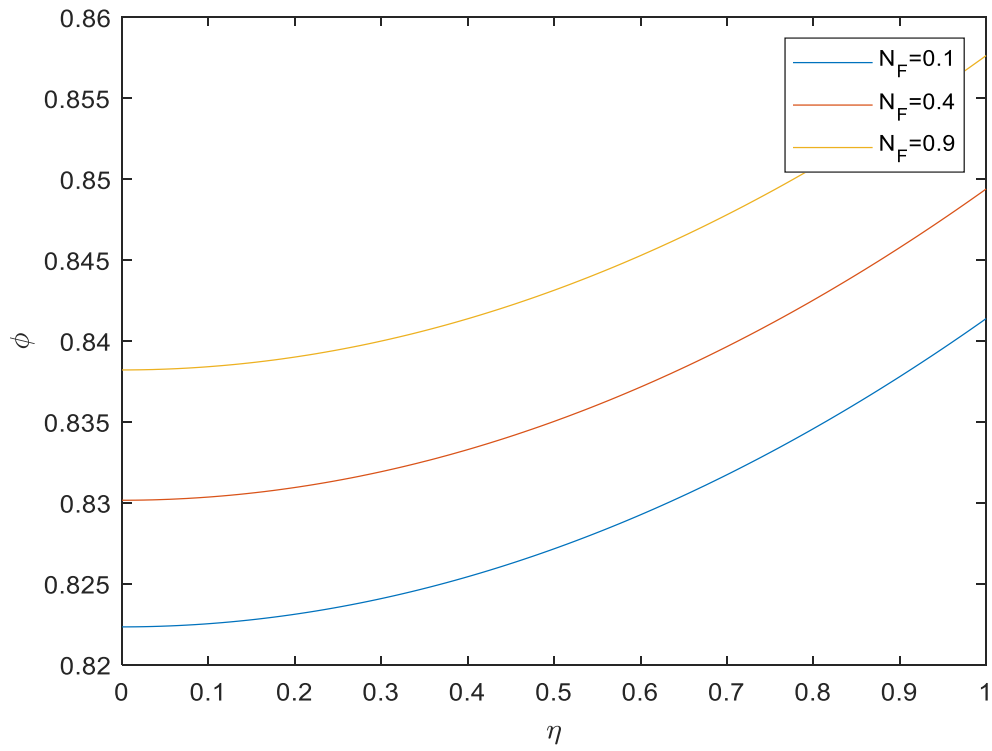

Figure 9. Concentration profiles at various Sr values.

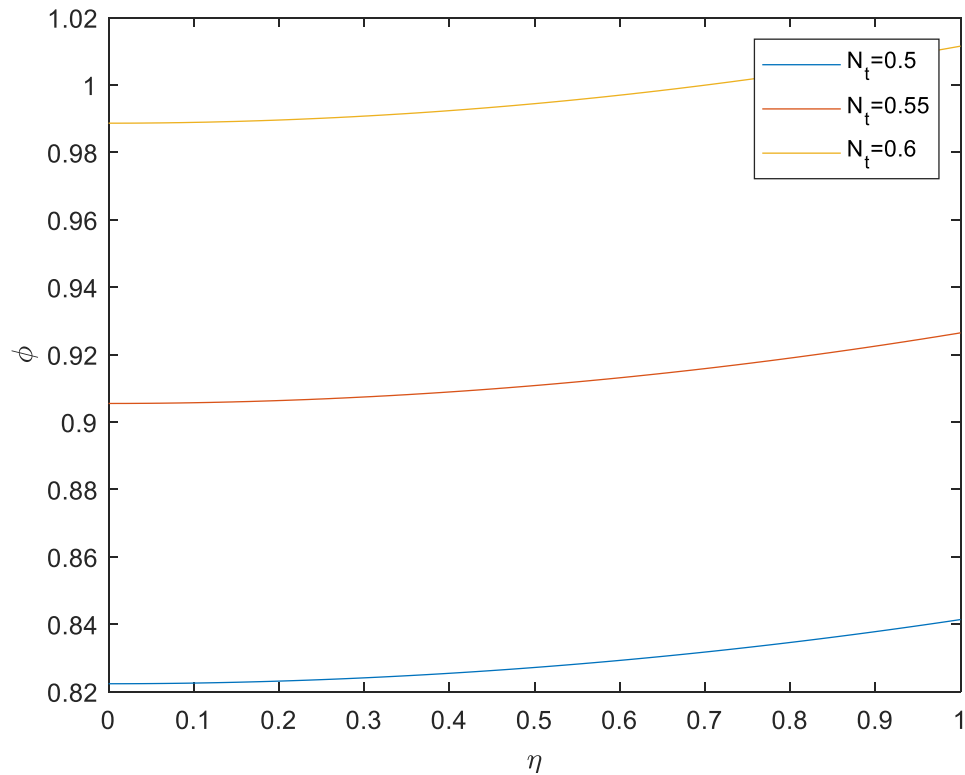**Figure 10.** Profiles of concentration for various N_F values.

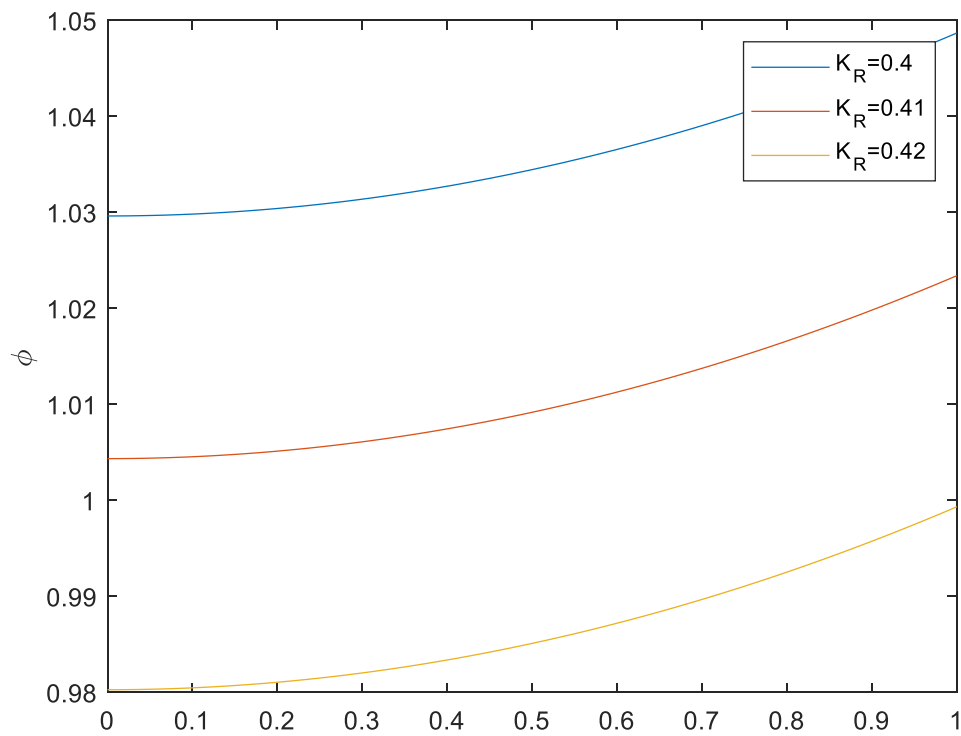

Figure 11. Profiles of concentration for numerous N_t values.

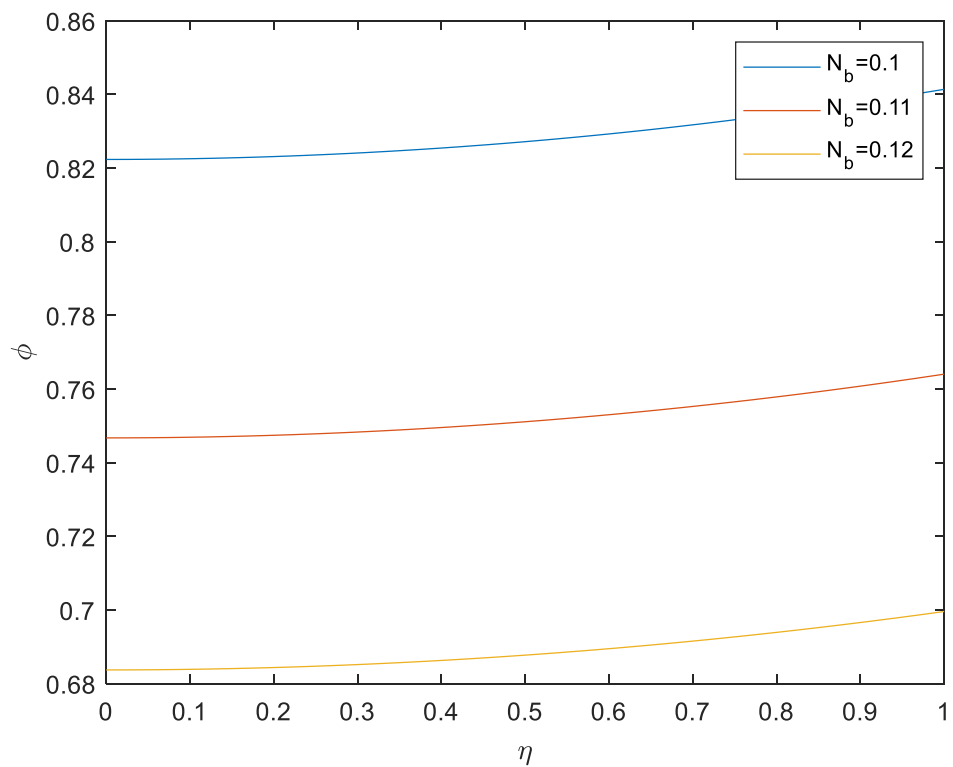**Figure 12.** Profiles of concentration for numerous K_R values.

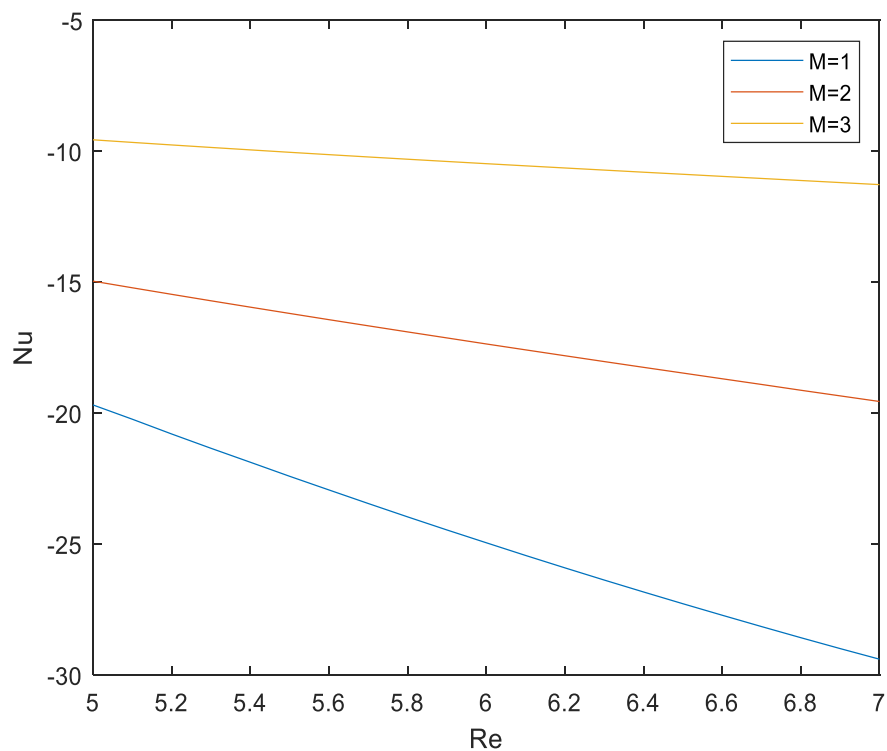**Figure 13.** Profiles of concentration for numerous N_b values.

Figure 14. Profiles of Nusselt numbers for various values of M.
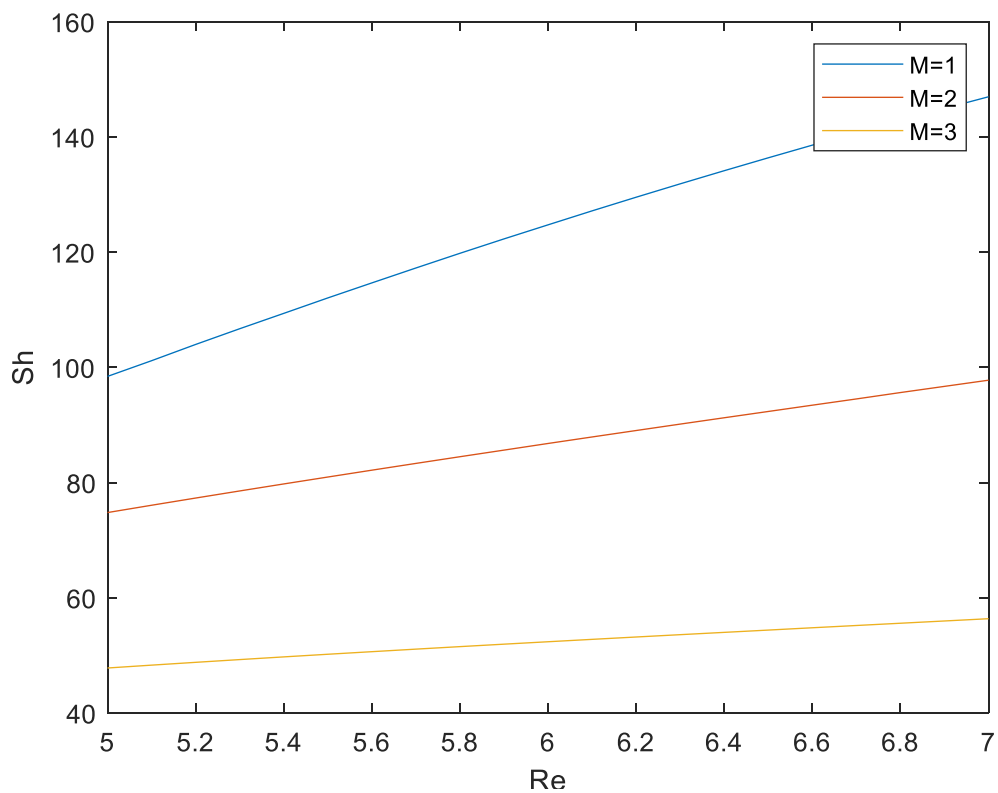

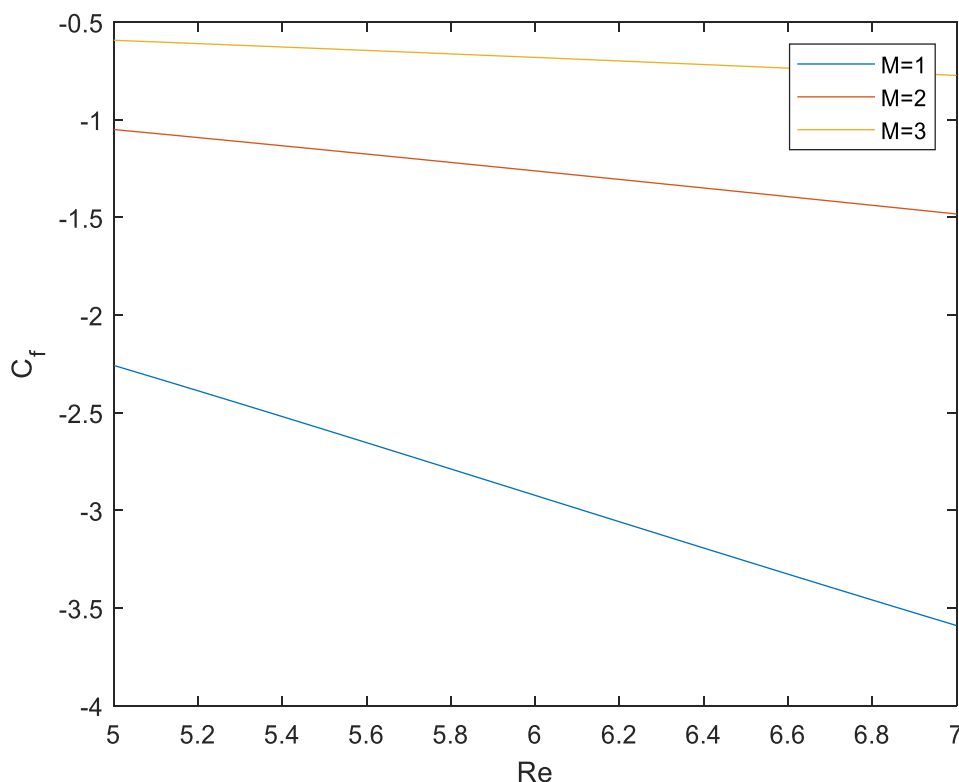**Figure 15.** Sherwood number profiles for various values of M.

Figure 16. Skin friction profiles for various values of M.

4) The Nusselt and Sherwood numbers, as well as skin friction, decrease as the magnetic field increases.

NOMENCLATURE

u, Velocity component in the radial direction (m/s); **c_p,** Heat capacity (kg/(m^3 K)); **B_o,** Magnetic field strength (T); **K,** The permeability constant of the porous medium (m^2); **T,** Temperature (K); A, Pressure gradient (Pa/m); C, Concentration; h, Coefficient of heat transfer (W/(m^2 K)); **F,** Forchheimer coefficient; **T_∞,** Ambient temperature (K); **D_T,** The thermophoresis diffusion coefficient (m^2/s); **D_B,** The Brownian diffusion coefficient (m^2/s); K_r, Dimensional chemical reaction parameter; **Re,** Reynolds number; **M,** Magnetic constraint; **N_b,** Brownian motion parameter; **N_F,** Porous medium resistance constraint; **Sc**, Schmidt number; **Ec,** Eckert number; **N_t,** Thermophoresis constraint; **K_R,** Chemical reaction constraint; **Pr,** Prandtl number; **Sr,** Soret number; **W,** Dimensionless velocity; **Bi,** Biot number; **N_p,** Porous medium shape parameter.Greek symbols: **p,** The fluid's density (kg/m^3); **σ,** Electrical conductivity (S/m); **k,** Thermal conductivity (S/m); μ, Dynamic viscosity (K); **v,** Kinematic viscosity (m^2/s); **φ,** Dimensionless concentration; **θ,** Dimensionless temperature.

CONFLICT OF INTERESTS

The authors have not declared any conflict of interests.

REFERENCES

Abdullah MR, Alghazawi OK, Al-Ayyad M (2019). Effect of Non-uniform Heat Source and Radiation on Transient MHD Flow Past a Vertical Moving Plate with Inclined Magnetic Field and Periodic Heat Flux Engineering, Technology & Applied Science Research 9(4):6.

Aly A, Chamkha A, Raizah Z (2020). Radiation and Chemical Reaction Effects on Unsteady Coupled Heat and Mass Transfer by Free Convection from a Vertical Plate Embedded in Porous Media. Journal of Heat and Mass Transfer Research 7(2):95-103.

Amidu MA, Addad Y, Riahi MK, Abu-Nada E (2021). Numerical investigation of nanoparticles slip mechanisms impact on the natural convection heat transfer characteristics of nanofluids in an enclosure. Scientific Reports 11(1):1-24.

Arifuzzaman S, Khan M, Mehedi M, Rana B, Ahmmed S (2018). Chemically reactive and naturally convective high speed MHD fluid flow through an oscillatory vertical porous plate with heat and radiation absorption effect. Engineering Science and Technology, an International Journal 21(2):215-228.

Arulmozhi S, Sukkiramathi K, Santra SS, Edwan R, Fernandez-Gamiz U, Noeiaghdam S (2022). Heat and mass transfer analysis of radiative and chemical reactive effects on MHD nanofluid over an infinite moving vertical plate. Results in Engineering 14:100-394. https://doi.org/10.1016/j.rineng.2022.100394.

Barik R, Dash G, Rath P (2018). Steady laminar MHD flow of visco-elastic fluid through a porous pipe embedded in a porous medium. Alexandria Engineering Journal 57(2):973-982.

Boukerma K, Kadja M (2017). Convective Heat Transfer of Al2O3 and CuO Nanofluids Using Various Mixtures of Water-Ethylene Glycol as Base Fluids. Engineering, Technology and Applied Science Research 7(2):1496-1503. https://doi.org/10.48084/etasr.1051.

Choi SU, Eastman JA (1995). Enhancing thermal conductivity of fluids with nanoparticles. Argonne National Lab.(ANL), Argonne, IL United States.

Das M, Mahanta G, Shaw S (2020). Heat and mass transfer effect on an unsteady MHD radiative chemically reactive Casson fluid over a stretching sheet in porous medium. Heat Transfer 49(8):4350-4369.

Dhanalaxmi DV (2015). Effects of Radiation, Heat Source/Sink, Viscous Dissipation on Unsteady MHD Fluid Flow over a Stretching Sheet. International Journal of Electronics Communication and Computer Engineering 6(3):6.

Elbashbeshy E, Abdelgaber KM, Asker H G (2018). Heat and mass transfer of a Maxwell nanofluid over a stretching surface with variable thickness embedded in porous medium. International Journal of Mathematics and Computer Science 4(3):86-98.

Haile E, Shankar B (2014). Heat and Mass Transfer in the Boundary Layer of Unsteady Viscous Nanofluid along a Vertical Stretching Sheet. Journal of Computational Engineering pp. 1-17. https://doi.org/10.1155/2014/345153.

Humane PP, Patil VS, Patil AB (2021). Chemical reaction and thermal radiation effects on magnetohydrodynamics flow of Casson–Williamson nanofluid over a porous stretching surface. Proceedings of the Institution of Mechanical Engineers, Part E: Journal of Process Mechanical Engineering 235(6):2008-2018.

Kandasamy R, Abd WR BM, Khamis AB (2006). Effects of chemical reaction, heat and mass transfer on boundary layer flow over a porous wedge with heat radiation in the presence of suction or injection. Theoretical and Applied Mechanics 33(2):123-148.

Keshtkar MM, Ghazanfari M (2017). Numerical Investigation of Fluid Flow and Heat Transfer Inside a 2D Enclosure with Three Hot Obstacles on the Ramp under the Influence of a Magnetic Field. Engineering, Technology and Applied Science Research 7(3):1647-1657. https://doi.org/10.48084/etasr.1115.

Khan MS, Mei S, Shabnam, Fernandez-Gamiz, U, Noeiaghdam S, Khan Aamir A (2022). Numerical simulation of a time-dependent electroviscous and hybrid nanofluid with Darcy-Forchheimer effect between squeezing plates. Nanomaterials 12(5):876. https://doi.org/10.3390/nano12050876.

Khan WA, Rashad AM (2017). Combined Effects of Radiation and Chemical Reaction on Heat and Mass Transfer by MHD Stagnation-Point Flow of a Micropolar Fluid Towards a Stretching Surface. Journal of the Nigerian Mathematical Society 36(1):20.

Khan W, Pop I (2010). Boundary-layer flow of a nanofluid past a stretching sheet. International Journal of Heat and Mass Transfer 53(11-12):2477-2483.

Kuznetsov A, Nield D (2010). Natural convective boundary-layer flow of a nanofluid past a vertical plate. International Journal of Thermal Sciences 49(2):243-247.

Mahabaleshwar U, Anusha T, Sakanaka P, Bhattacharyya S (2021). Impact of inclined Lorentz force and Schmidt number on chemically reactive Newtonian fluid flow on a stretchable surface when Stefan blowing and thermal radiation are significant. Arabian Journal for Science and Engineering 46(12):12427-12443.

Makinde OD, Khan ZH, Ahmad R, Haq R U, Khan WA (2019). Unsteady MHD Flow in a Porous Channel with Thermal Radiation and Heat Source/Sink. International Journal of Applied and Computational Mathematics 5(3):59. https://doi.org/10.1007/s40819-019-0644-9.

Mjankwi MA, Masanja VG, Mureithi EW, James MN (2019). Unsteady MHD Flow of Nanofluid with Variable Properties over a Stretching Sheet in the Presence of Thermal Radiation and Chemical Reaction. International Journal of Mathematics and Mathematical Sciences 2019:1-14. https://doi.org/10.1155/2019/7392459.

Muyungi WN, Mkwizu MH, Masanja VG (2022). The Effect of Navier Slip and Skin Friction on Nanofluid Flow in a Porous Pipe. Engineering, Technology and Applied Science Research 12(2):8342-8348. https://doi.org/10.48084/etasr.4763.

Nayak MK, Dash GC, Singh LP (2016). Heat and mass transfer effects on MHD viscoelastic fluid over a stretching sheet through porous medium in presence of chemical reaction. Propulsion and Power Research 5(1):70-80.

Obulesu M, Raghunath K, Charankumar G, Ramu S, Giulio L. (2021). MHD Heat and Mass Transfer Steady Flow of a Convective Fluid Through a Porous Plate in The Presence of Diffusion Thermo and Aligned Magnetic Field. Journal of Advanced Research in Fluid Mechanics and Thermal Sciences 89(1):62-76. https://doi.org/10.37934/arfmts.89.1.6276.

Rao S, Deka P (2023). A Numerical Study on Unsteady MHD Williamson Nanofluid Flow past a Permeable Moving Cylinder in the presence of Thermal Radiation and Chemical Reaction. Biointerface Research in Applied Chemistry 13(5):436.

Reddy GB, Goud BS, Shekar M (2019). Numerical solution of MHD mixed convective boundary layer flow of a nanofluid through a porous medium due to an exponentially stretching sheet with magnetic field effect. International Journal of Applied Engineering Research 14(9):2074-2083.

Sadighi S, Jabbari M, Afshar, H, Danesh Ashtiani HA (2022). MHD heat and mass transfer nanofluid flow on a porous cylinder with chemical reaction and viscous dissipation effects: Benchmark solutions. Case Studies in Thermal Engineering 40:102443. https://doi.org/10.1016/j.csite.2022.102443.

Saeed A, Rehan AS, Muhammad SK, Unai FG, Mutasem ZBF, Samad N, Ahmed MG (2022). Theoretical analysis of unsteady squeezing nanofluid flow with physical properties. Mathematical Biosciences and Engineering 19(10):10176-10191. https://doi.org/10.3934/mbe.2022477.

Sharma M, Bhupendra KS, Umesh Khanduri NK, Mishra SN, Fernandez-Gamiz U (2023). Optimization of heat transfer nanofluid blood flow through a stenosed artery in the presence of Hall effect and hematocrit dependent viscosity. Thermal Engineering 47:103075. https://doi.org/10.1016/j.csite.2023.103075.

Sheremet MA, Öztop H F, Abu-Hamdeh N, Bondareva NS (2018). Transient natural convection in a partially open trapezoidal cavity filled with a water-based nanofluid under the effects of Brownian diffusion and thermophoresis. International Journal of Numerical Methods for Heat and Fluid Flow 28(3):606-623. https://doi.org/10.1108/HFF-04-2017-0170.

Zubaidah S, Kechil SA (2019). Steady Magnetohydrodynamic flow of Third-Grade Non-Newtonian Nanofluid in Porous Coaxial Cylinders. ASM Science Journal. https://doi.org/10.32802/asmscj.2020.sm26(4.20).